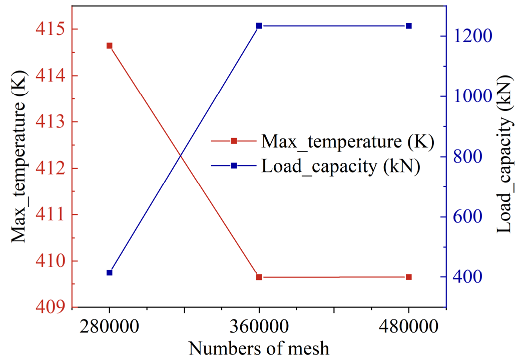

Figure S1. *mesh independence verification*

To ensure the accuracy of the numerical results, a mesh independence study was conducted with three mesh schemes. Taking the maximum oil film temperature and load-carrying capacity as verification indicators, when the mesh number increases from 360000 to 480000, the relative deviations of both indicators are less than 1%. Considering both computational accuracy and efficiency, the medium mesh scheme with 480000 elements was finally adopted. The mesh independence verification is presented in Fig. S1.

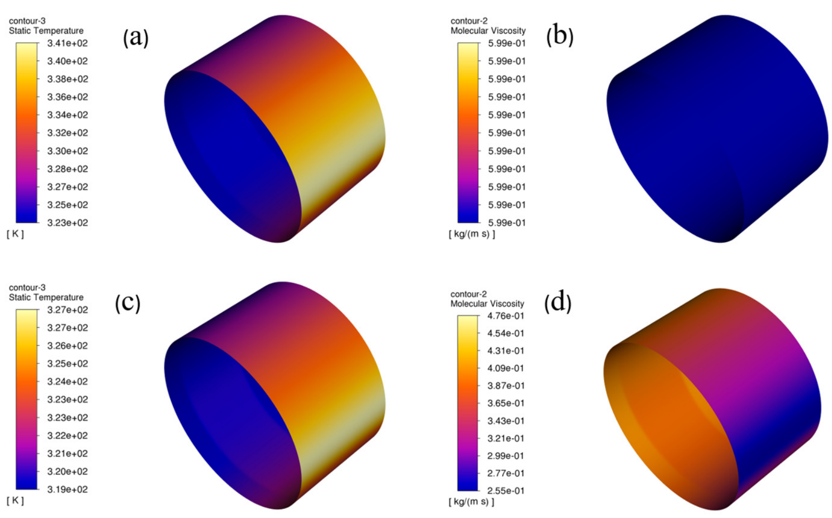

Figure S2. *Contour of oil film temperature and viscosity fields for VG680 lubricant at 30 rpm: (a) Viscosity field under TVCM; (b) Viscosity field under CVM; (c) Temperature field under TVCM; (d). Temperature field under CVM*

Figure S2 presents contour maps of the oil-film temperature and viscosity fields of VG680 lubricant predicted by the CVM and TVCM, further highlighting the limitations of the CVM. Under the CVM, the viscosity throughout the oil-film region remains fixed at the initial value of 0.599 Pa·s, completely failing to capture the temperature-induced viscosity gradient. In contrast, the TVCM predicts a pronounced localized viscosity decrease: in the converging wedge region of the oil film (the minimum-film-thickness region), the viscosity drops to 0.298 Pa·s, forming an obvious gradient from the inlet side toward the high-shear region. This dynamic viscosity variation directly alters the local flow resistance and shear-stress distribution, thereby regulating heat generation as well as convective and diffusive heat transfer, and ultimately producing a nonlinear coupled thermo-viscous multi-field effect.

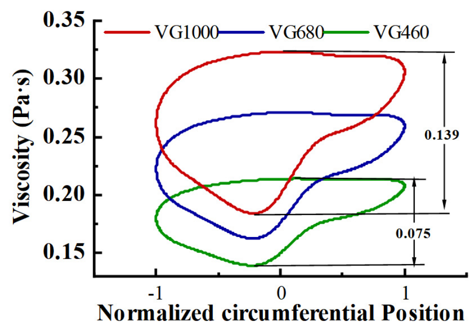

Figure S3. *Circumferential viscosity distribution at 50 rpm*

To further investigate the distribution of the oil film viscosity field, figure S3 presents the circumferential viscosity distribution at the centerline for lubricating oils of different viscosity grades at 50 rpm. It can be seen that the maximum circumferential viscosity difference increases with the initial viscosity grade of the lubricant. This trend indicates that a higher initial viscosity corresponds to greater viscosity-temperature sensitivity, leading to a more pronounced non-uniformity in the oil film viscosity distribution.

This phenomenon can be explained by combining the earlier analysis of the temperature field. The primary reason is that within the wedge-shaped convergent region, the oil film is thin and experiences a high shear rate. This causes a sharp temperature rise, which in turn leads to a significant local reduction in viscosity. Furthermore, a higher initial viscosity results in a greater amplitude of viscosity attenuation and more distinct local gradient variations. Ultimately, this intensifies the circumferential viscosity difference across the oil film.

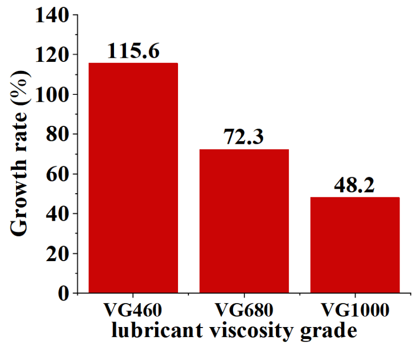

Figure S4. *Comparison of viscous forces at 10 rpm and 50 rpm*

Figure S4 shows the calculated growthzengzhanglü rates of viscous force for three lubricants within the speed range of 10 – 50 rpm. The corresponding growth rates are 115.6% for VG460, 72.3% for VG680, and 48.2% for VG1000, respectively. The results quantitatively demonstrate that the growth rate of viscous force decreases monotonically as the lubricant viscosity increases. This difference is caused by the stronger thermal thinning effect of high-viscosity lubricants, which offsets the increase in shear stress induced by elevated rotational speed.

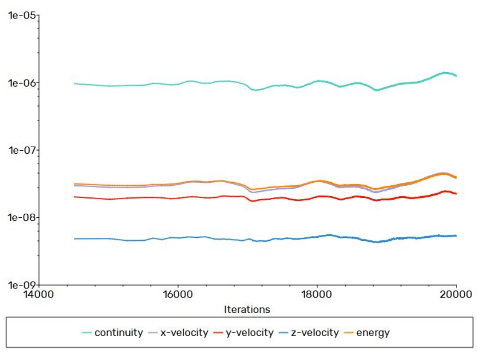

(a)

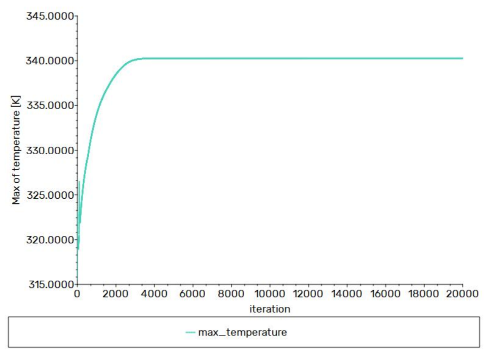

(b)

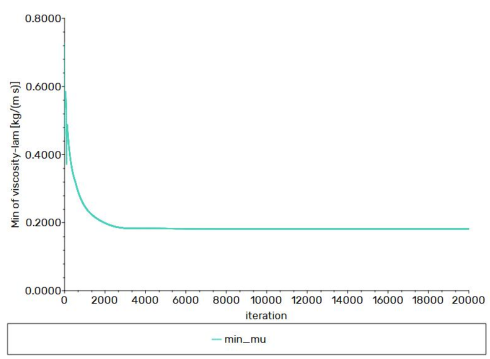

(c)

Figure S5.Residual evolution curves and monitored profiles of key parameters for the representative case of VG1000 lubricant operating at 50 rpm:
(a) Residual curves; (b) maximum temperature; (c) minimum dynamic viscosity

To eliminate the risk of pseudo-convergence and verify the reliability of the iterative solution process, Figure S5 illustrates the residual evolution curves and key parameter monitoring profiles for the representative case of VG1000 lubricant at 50 rpm. This case is specifically selected as it represents the most challenging scenario—combining the highest lubricant viscosity with the highest rotational speed—where thermo-viscous coupling iterations are most difficult to converge. The results demonstrate that all equation residuals drop below the prescribed threshold and that the monitored maximum oil film temperature, minimum dynamic viscosity, and load-carrying capacity remain stable without continuous drift, thereby guaranteeing reliable convergence across all other operating conditions.

Table S1. Load-carrying capacity of three lubricants at different rotational speeds

Rotational Speed (rpm)	***VG460 load-carrying capacity (N)***	***VG680 load-carrying capacity (N)***	***VG1000 load-carrying capacity (N)***
10	*109418*	*162222*	*218459*
20	*184919*	*256874*	*327383*
30	*227272*	*299823*	*368250*
40	*249343*	*316736*	*379628*
50	*260192*	*322095*	*379202*

The load-carrying capacities and their corresponding growth rates of VG460, VG680 and VG1000 lubricants at two rotational speed ranges (10 – 30 rpm and 30 – 50 rpm) are presented as follows.

Speed range: 10 – 30 rpm

VG1000: Load-carrying capacity increases from 218 kN to 368 kN, with a growth rate of 68.6%;

VG680: Load-carrying capacity increases from 162 kN to 300 kN, with a growth rate of 84.8%;

VG460: Load-carrying capacity increases from 109 kN to 227 kN, with a growth rate of 107.7%.

Speed range: 30 – 50 rpm

VG1000: Load-carrying capacity increases from 368 kN to 379 kN, with a growth rate of 3.0%;

VG680: Load-carrying capacity increases from 300 kN to 322 kN, with a growth rate of 7.3%;

VG460: Load-carrying capacity increases from 227 kN to 260 kN, with a growth rate of 14.5%.